

# Constant-Flux Edge Sensor

Alexei Filatov\* and Larry Hawkins  
Calnetix Technologies  
Cerritos, USA

## Abstract

A novel axial position sensor is presented. The sensor offers a unique combination of advantageous properties not found collectively in other axial position sensing solutions. These include ability to work in dusty environments and in many working fluids, low sensitivity to temperature as well as external electrical and magnetic fields, good linearity over a large displacement range, large intrinsic gain, easy integration into a machine, robustness to the variations in parameters of the external wiring, simplicity of the signal processing electronics, sufficient frequency bandwidth and a commonality of used elements with radial magnetic reluctance position sensors. This paper describes the operating principle, test procedure and test results of the constant-flux edge sensor in both single-sided and differential configurations. Presently the sensor has been successfully integrated into several commercial machines and extensively tested under various operating conditions.

## 1 Introduction

Position sensors are critical components of any Active Magnetic Bearing (AMB) [1]. Their role is to continuously provide the controller with accurate up-to-date information about the rotor position unaffected by external factors such as speed, temperature, dust, working fluids, external magnetic and electrical fields, etc. Even though a significant progress has been made in developing self-sensing AMBs [2], in which functions of the position measurement and the force generation are combined in one physical component, their fundamental performance limitations will likely limit their use to low-cost low-speed machines and a conventional arrangement utilizing dedicated radial and axial sensors will remain dominant.

Figure 1 shows a typical configuration of a rotating machine (e.g. a turbocompressor) on magnetic bearings with dedicated position sensors. Two sets of radial position sensors installed on the opposite ends of the rotor are providing information about radial displacements of the corresponding rotor ends, whereas the axial position sensor provide the information about the rotor axial displacement. Permanent magnet biased homopolar radial and combination (radial and axial) actuators are shown as an example, however, any other type of electromagnetic actuators can be used to generate forces necessary to support the rotor without a mechanical contact. When magnetic bearing are not operational, the rotor rests on backup bearings: front set of backup bearing provides axial and radial rotor support, whereas the rear set only provides the radial support of the rear rotor end.

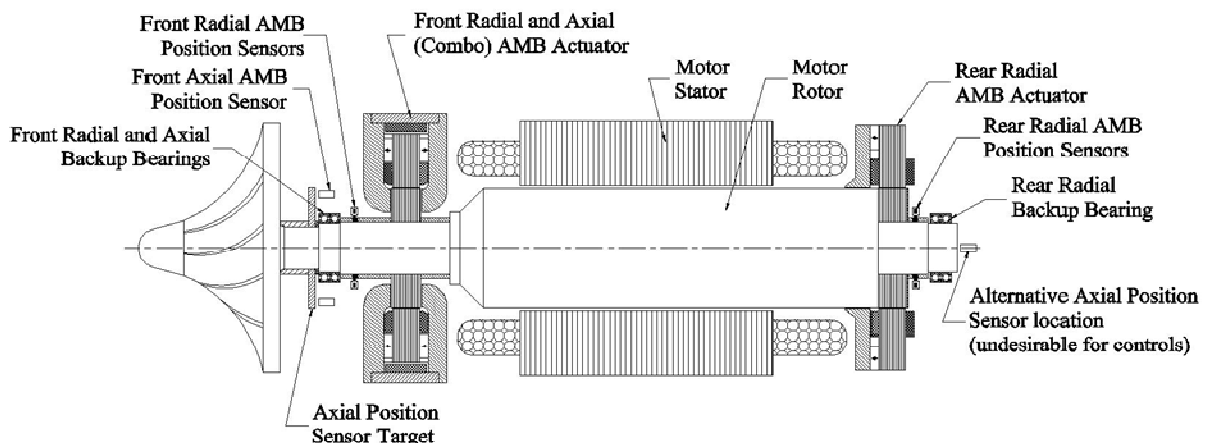


Figure 1: A typical layout of a rotating machine on active magnetic bearings (e.g. a turbocompressor).

\*afilatov@calnetix.com, 16323 Shoemaker Av, Cerritos, CA, 90703, ph: +1.562.293.1667, f: +1.562.293.1689

When choosing a location for the axial position sensor, it is important to remember that in Active Magnetic Bearing systems the controls work to maintain relative rotor-stator alignment where the axial sensor is located. Because of this, the axial sensor location on the front end of the machine in this example close to the axial (combo) actuator, the axial backup bearing and the impeller is better than the alternative position with the axial sensor looking at the rear face of the rotor: when the machine temperature varies, the changes of the important axial clearances between rotating and stationary parts of the actuator, backup bearings and impeller due to differences in thermal expansions will not vary in the first case nearly as much as in the second.

Different types of position sensors have different combinations of properties making some of them more suitable for a given application than the other. In the industrial environment, however, it is typically preferable to have one technology that would cover as many applications as possible. From a wide variety of the available technologies, including optical, capacitive, and electromagnetic position sensors, the latter appear to be the most universal solution [1].

The electromagnetic sensors fall into two categories: inductive (reluctance) sensors and eddy-current sensors. The inductive sensors [3] utilize a closed magnetic circuit formed by a soft-magnetic, preferably electrically non-conductive stationary core and a sensor target mounted on the object which position is being measured. The stationary core and the sensor target are separated by an air gap. Instead of using a soft-magnetic but electrically non-conductive material, the sensor head cores and the sensor target are often assembled from electrically isolated laminations of electrical steel stuck together in the axial direction. The position measurements are based on measurements of inductances of sensor coils wound around the stationary cores. Changes in the rotor position result in changes of the magnetic reluctance of the air gap, and, consequently, changes in the inductance of a coil wound around the stationary portion of the magnetic circuit. These changes in the inductance are subsequently converted into the sensor output signal by sensor electronics.

The operational principle of the eddy-current sensors [4], [5] is similar to that of the inductive sensors, but the sensor target is made highly-conductive, and preferably, non-magnetic. An AC magnetic flux generated by a sensor coil induces eddy currents in the sensor target, which, in turn, affects the coil inductance. Since this effect depends on the distance between the sensor core and the sensor target, changes in the position of the sensor target result in changes of the coil inductance, similar to the inductive sensors. In order to maximize sensitivity to the target position and simplify the construction, eddy-current sensors in most cases do not have soft-magnetic cores. With no core, and with a non-magnetic target, the inductance of an eddy-current sensor coil is typically a small fraction of an inductance of an inductive sensor. This inductance is further reduced by the presence of the eddy currents in the sensor target.

Because of small inductances, in order to obtain a necessary signal-to-noise ratio without exceeding current limits in the sensor coil, the eddy-current sensors are typically operated at much higher frequencies than the inductive sensors (approximately 500kHz to 2MHz for the eddy-current sensors versus 1 to 100kHz for the inductive sensors). Small inductance of the eddy-current sensors complicates their usage in magnetic bearing systems because the impedance of the wires connecting the sensor coil to the sensor electronics often becomes comparable with the inductance of the sensor coil. As a result any changes to the wires length, adding an additional connector, or even changing how the wires are routed in space may have effect on the sensor readings [5]. Furthermore, electronics for processing higher-frequency signals used by the eddy-current sensors is more complicated and expensive than electronics for the inductive sensors.

Alternative designs of the eddy-current sensors are also known [6], however, while offering the cost and manufacturability advantages they still require very high operational frequency.

Since the axial position sensor presented here was developed on the basis of inductive (magnetic reluctance) sensors, in this introduction we will briefly discuss specifics of their applications in rotating machines on active magnetic bearings in order to highlight the technology drawbacks that we attempted to address with this development. We will also draw some comparisons with eddy-current sensors, which are closely related to the magnetic reluctance sensors based on their operational principle.

An identical geometrical radial sensor arrangement can be implemented with eddy-current sensors, even though the signal processing normally would be somewhat different in this case.

Figure 2 shows a typical arrangement of inductive sensors to measure radial displacements of a rotor in X and Y directions. This arrangement includes two sensor heads per measurement axis located along the axis diametrically opposite to each other in the proximity of the sensor target (for example sensor heads LY2 and LY1 are used to measure the rotor displacement along the Y axis). In one of the common signal processing schemes, shown here as an example, windings of the sensors associated with a particular axis are connected in series forming a voltage divider and energized with an AC voltage of a fixed amplitude. If the sensor target is shifted for example towards the LY2 sensor (positive Y direction), the inductance of this sensor winding will become bigger, whereas the

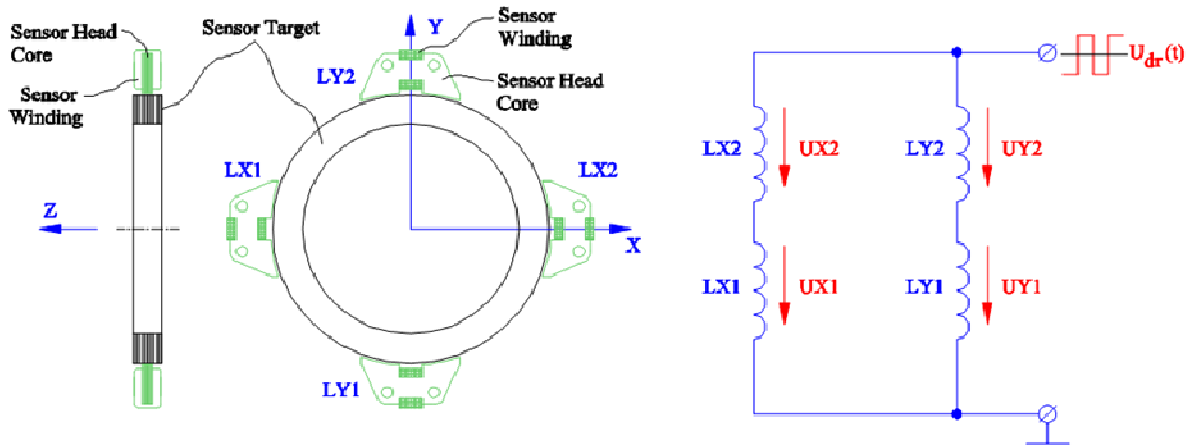


Figure 2: An example of a conventional arrangement of inductive sensors to measure radial displacements of a sensor target.

inductance of the sensor winding LY1 will become smaller. As a result, voltage drop on the LY2 sensor winding UY2 will become bigger than the volt drop UY1 on the LY1 sensor. After demodulation, the voltage difference UY2-UY1 can be used as a measure of the rotor displacement in the Y direction.

Figure 3a provides a close up detailed view of the axial sensor arrangement shown in Figure 1 along with an illustration of a typical signal processing principle. When the sensor target disk moves axially, inductances of the sensor heads LZa and LZb change synchronously by approximately the same amount. Consequently, this changes the voltage drop UZ measured across both sensor heads LZa and LZb in a voltage divider they form with an external inductance LZref.

Two diametrically opposite sensor heads LZa and LZb are used instead of one in order to minimize effects of the sensor target tilt on the sensor readings: changes of the inductances LZa and LZb caused by the sensor target tilt will be opposite in sign and almost equal in magnitude, therefore the sum of the inductances LZa and LZb will stay about the same.

An inherent advantage of this sensor design is its tolerance to the radial rotor displacement – such displacements do not change inductances LZa, LZb, and, consequently, do not introduce errors, as long as their faces remain fully covered with ample margins by the sensor target.

The reference inductor can be made external to the machine, but in this case the sensor might exhibit a large

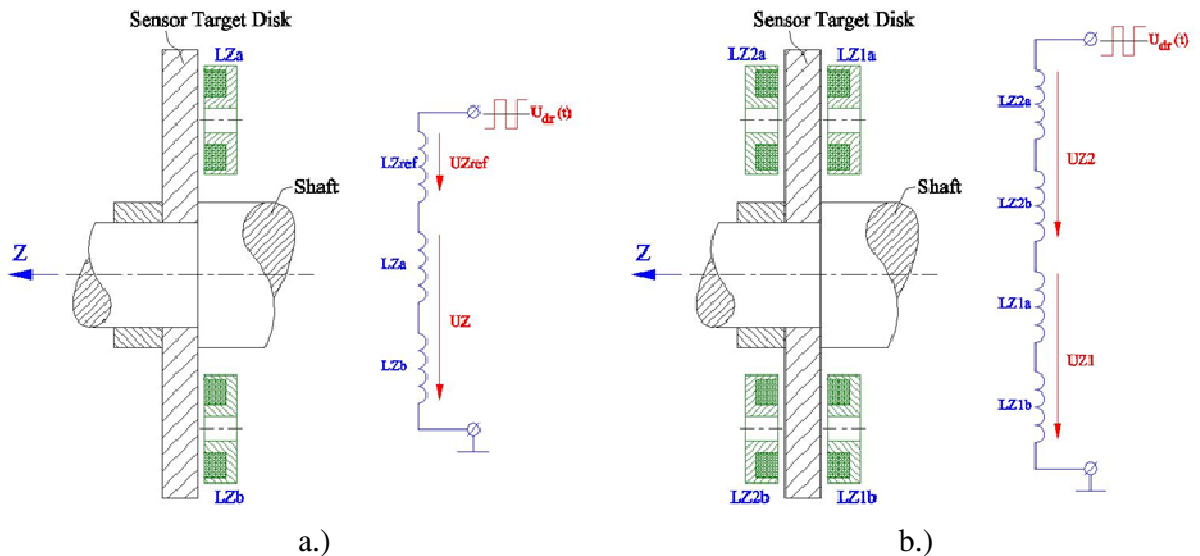


Figure 3: An example of one of conventional arrangements of inductive sensors to measure axial displacements of a sensor target. a.) single-sided configuration, b.) differential configuration.

thermal error because the inductor value is likely to be temperature dependent. Ideally, to minimize thermal errors the reference inductor should be identical in construction to the inductors LZa and LZb, look at a sensor target made of material identical to that of the sensor target for LZa-LZb and be located very close to them inside of a machine in order to be exposed to the same temperature.

From the axial sensor performance point of view, it would be better to use a differential sensor arrangement shown in Figure 3b with two sensor pairs LZ1a-LZ1b and LZ2a-LZ2b looking at the opposite axial faces of the sensor target. Effectively the sensor pair LZ2a-LZ2b would replace the reference inductor LZref in Figure 3a, but their net inductance instead of being constant would change in counterphase with the inductance of the pair LZ1a-LZ1b. As a result, the overall gain of the sensor arrangement shown in Figure 3b would be twice the gain of the sensor arrangement shown in Figure 3a, but the main benefits would be its intrinsic thermal stability and greater linearity.

Despite of all the advantages of the differential sensor arrangement shown in Figure 3b over the single-sided arrangement shown in Figure 3a, it is almost never used in commercial applications due to assembly difficulties caused by having the sensor target disk sandwiched between two stationary sets of the sensor heads.

One fundamental problem with the axial position sensing technology presented in Figures 3a and 3b is that it requires a surface orthogonal to the rotational axis of the machine. In most cases, such surface is not present at the desirable location and an additional component needs to be added to the rotor (such as the sensor target disk in Figure 1), which negatively affects rotordynamic performance, complicates assembly, increases cost and reduces reliability. Note that, as discussed earlier, using a flat end of the shaft located on the opposite end from the components that require precise positioning of the rotor portion with respect to the stator portion (such as axial (combo) magnetic bearings, axial backup bearings, unshrouded impellers, etc.) is not normally desirable due to the thermal expansion issues. There are few exceptions, however, where a sensing surface is present at the right location from the beginning, but they constitute a rather small fraction of all machines on magnetic bearings [7-9].

Another fundamental problem with this approach is a limited sensor frequency bandwidth caused by practical difficulties with making the sensor target non-conductive or laminated in the axial plane. Without these measures, the eddy-currents induced in a conductive target will have an effect on the sensor inductance opposite to the effect of changing the air gap in an inductive sensor, resulting in a reduced sensor gain. The higher excitation frequency, the larger would be the eddy-current effect, and the lower would be the sensor gain.

Eddy-current sensors can be used instead of the reluctance sensors in configurations shown in Figures 3a and 3b in a similar fashion, but their will have an advantage of a higher bandwidth, since eddy currents in the target enable their operation rather than negatively affecting it as in reluctance sensors.

Figure 4a illustrates another approach to the axial sensor design, which is almost identical to the radial sensor arrangement shown in Figure 2, but having the sensor heads LZ1 and LZ2 located at an edge of the sensor target

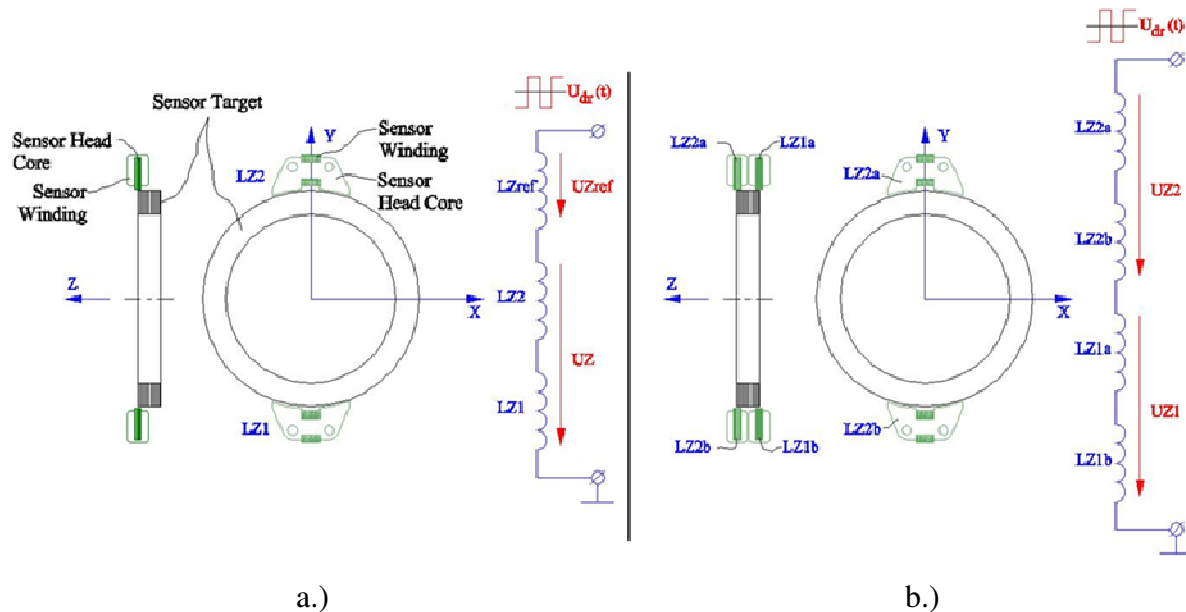


Figure 4: An example of another commonly used conventional arrangement of inductive sensors to measure axial displacements of a sensor target. a.) single-sided configuration, b.) differential configuration.

rather than in the middle of the target. Because this sensor is effectively monitoring the axial position of the edge of the sensor target it is commonly referred to as an edge sensor. The inductances of two sensor heads LZ1 and LZ2 change synchronously when the rotor moves axially, because this changes the area of overlapping between the sensor head cores and the outer surface of the sensor target. Note that this is different from designs shown in Figures 2, 3a and 3b where the inductances were changing because of the changes of the distances between the sensor heads and the sensor targets.

The inductances of individual heads LZ1 and LZ2 in Figure 4a also change in the same fashion as in designs shown in Figures 2, 3a and 3b (through changes of the distances between the sensor heads and the sensor targets) when the sensor target is displaced radially in the Y-direction, but these changes of inductances LZ1 and LZ2 happen in the opposite phases and their effects on the output signal to some degree cancel each other. For example, when the sensor target moves in the positive Y direction, the inductance of the sensor LZ2 increases, but the inductance of the sensor LZ1 decreases, and vice versa. Therefore, in the linear approximation, the sum of the inductances LZ1 and LZ2 is not affected by radial displacements of a rotor. In reality, however, changes of the inductances are not linear functions of the radial displacements, and the axial sensors such as shown in Figure 4a exhibit significant errors when the rotor is displaced radially. Figure 7a gives an example of such error magnitude observed in a real machine with an edge sensor. Such errors can be accounted for if the rotor radial position is known, but, nevertheless, this complicates the use of the sensor.

Another drawback of this arrangement is much smaller raw sensor gain compared to the arrangement shown in Figure 3a. Of course, the gain can be boosted by the signal processing electronics, but when the useful input signal to that electronics is small, it will be more affected by the electromagnetic noise, whereas the electronics will amplify both the useful signal and the noise.

The sensor configuration shown in Figure 4a can also be implemented in a differential form as illustrated in Figure 4b. In contrast to the differential implementation of the sensor arrangement per Figure 3a shown in Figure 3b, it does not make the machine assembly more difficult – the shaft simply slides through the stationary part in either single-sided configuration (Figure 4a) or the differential one (Figure 4b). The differential arrangement per Figure 4b would have twice the gain, much smaller thermal error and a more linear response than the single-sided arrangement shown in Figure 4a, but it also would be more expensive and would take more axial space.

An additional practical benefit of using the axial sensing scheme shown in Figures 4a and 4b is that it may use exactly the same sensor heads as in the radial sensing arrangement shown in Figure 2, thus reducing the part count in the machine. Furthermore, the axial edge sensor as in Figures 4a and 4b and the radial sensor as in Figure 2 can be combined in one housing and use a common sensor target thus forming a combination radial-axial inductive position sensor shown in Figure 5.

While the arrangement shown in Figures 3a and 3b worked well with an eddy-current sensor instead of the inductive sensors, the arrangements shown in Figures 4a and 4b would be much more difficult to realize with the

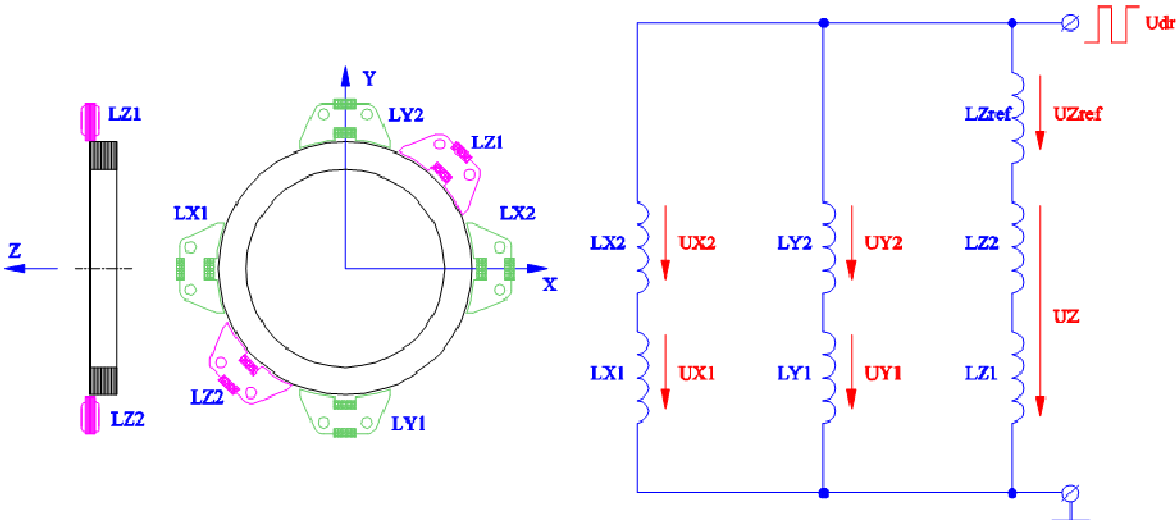


Figure 5: An example of a combination inductive sensor arrangement providing both radial and axial position measurement of a sensor target.

eddy-current sensors because the magnetic flux would not be guided by soft-magnetic structures, and, therefore, there would be no well-defined “electromagnetic edge” on the rotor.

Probably the biggest drawback of the inductive sensors for applications in AMBs is their sensitivity to external magnetic field attracted to the soft-magnetic core of the sensor. Whereas it is typically desirable to locate sensors close to the corresponding actuators to have a more accurate positioning of the actuator target in the nominal position, this may cause strong magnetic fields produced by the actuator to affect the sensor readings. The effect becomes especially dangerous in machines with soft-magnetic shaft which are very effective in conveying the magnetic fields between various system components.

Figure 6 illustrates this by an example of a radial or an axial edge sensor used in combination with a “Combo” AMB actuator [10] exerting both axial and radial forces on a rotor. The “dashed” line on the left represents a leakage field from the actuator into the sensor. This field affects the operating point of the sensor core material on the BH curve, and, therefore, influences the sensor inductance and, consequently, the position readings. When the axial control flux is varied in order to produce the axial force required from the actuator, the leakage flux varies as well. This results in sensor errors dependent on the axial control current in the actuator.

The right part of the Figure 6 shows leakage flux density within the sensor head calculated with 3D FEA for the worst-case-scenario. Note that only the leakage field is shown, not the excitation field which is expected to be present in the sensor head during the operation. The leakage flux density in the sensor head turned out to be surprisingly high (in excess of 1.3T in many places) and clearly could affect the sensor operation.

In the radial sensor arrangement shown in Figure 2 the effect of the leakage field is mitigated by using two diametrically opposite differentially connected sensor heads: the inductance change for each sensor head due to the leakage field would be the same as the inductance change for the diametrically-opposite head, and, therefore, the output of the voltage divider will not change as long as the rotor is maintained close to the the central position.

In case of the axial sensors, on the other hand, even if two differentially connected sensors located on the axially opposite sides of the sensor target were used as shown in Figure 4b, their changes in the inductance due to the leakage fields will not cancel each other because the differential sensor head pairs LZ1a-LZ1b and LZ2a-LZ2b will be located at different distances from the actuator, and, therefore, will be exposed to different leakage fields. Moreover, the sensor heads LZ1a-LZ1b located closer to the actuator would absorb most of the field, effectively shielding the sensor heads LZ2a-LZ2b.

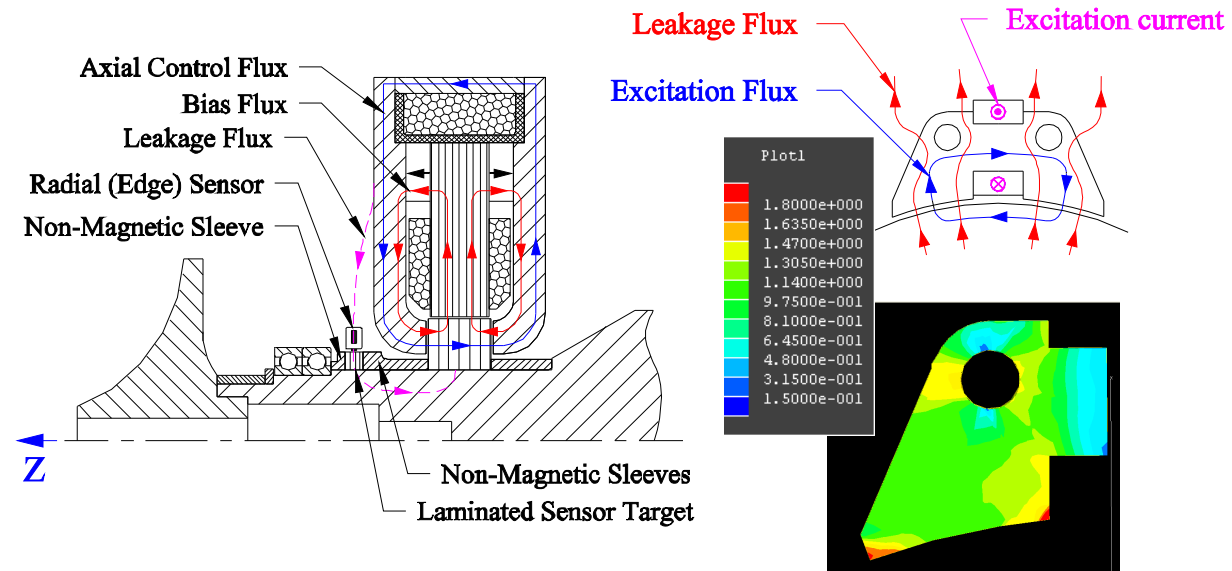


Figure 6: Illustration of a magnetic flux leakage from an electromagnetic actuator (e.g. a homopolar PM-biased combination bearing) into an inductive position sensor head.

Figure 7b illustrates an axial position measurement error observed when testing an edge sensor as a function of the external magnetic flux density measured in the air gap between the sensor head poles and the sensor target.

The new axial inductive sensor – constant-flux edge sensor – presented in this paper is developed to address drawbacks of the existing inductive and eddy-current axial sensors. It offers a unique combination of advantageous properties not found collectively in other axial position sensing solutions, including:

1. Ability to work in dusty environments and in many working fluids.
2. Low sensitivity to external leakage fields.
3. Low sensitivity to radial rotor displacements.
4. Low sensitivity to temperature variations.
5. Large temperature operating range (up to 175°C tested, up to 250°C theoretically possible).
6. Excitation frequency in the ranges where impedance of the external wiring can be neglected, but the sensor bandwidth is sufficient for AMB applications (we use 25-50kHz excitation frequency).
7. Raw gain above 4.0 V/mm.
8. Very large total measurement range (in excess of 5mm).
9. Sufficiently large linear subranges (at least 0.75mm) where the gain variation does not exceed +/-20%.
10. No requirements for a sensor target surface normal to the Z-axis.
11. Commonality with the radial sensor design.

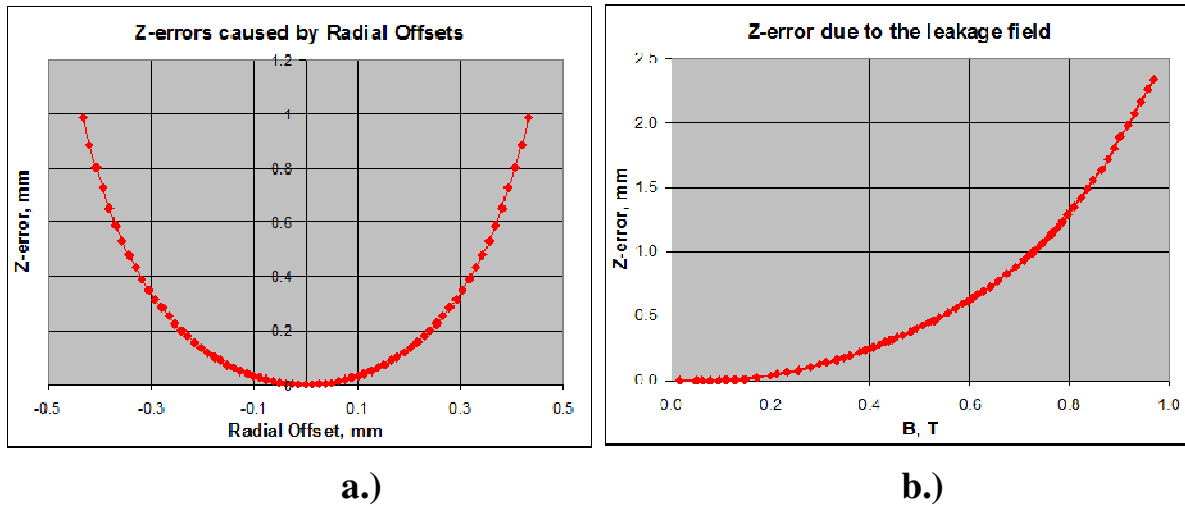


Figure 7: Conventional edge sensor axial position measurement errors caused by a.) radial rotor offsets and b.) leakage magnetic fields. The leakage field values shown on the graph were measured in the air gap between a pole of the sensor head and the laminated sensor target.

## 2 Operating principle of the Constant-Flux Edge Sensor

The key idea behind the constant-flux edge sensor design is to use magnetic flux distribution in an air gap rather than the coil impedance as a measure of the axial position of the rotor. For example, if we assume that somehow the total magnetic flux in the air gap between a sensor head (e.g. sensor head LZ1) in Figure 4a and the sensor target is maintained constant, then the flux density at each point of the air gap will change when the sensor target is displaced axially. Therefore, by measuring flux density at a certain point, or an average flux density over a certain part of the air gap, one could estimate the axial displacement of the rotor.

Figure 8 further clarifies this idea. The total flux injected into the air gap between the sensor head core and the sensor target is represented by five flux lines and is maintained constant regardless the axial position of the sensor target (how to implement this constant-flux requirement will be discussed later). As shown in Figure 8, the flux density above the actuator target changes when the target is displaced axially from the nominal position shown in Figure 8a: the space between the flux lines gets smaller (flux density gets higher) when the sensor target moves in the negative Z direction (Figure 8b) and, conversely, the space between the flux lines gets larger (flux density gets lower) when the sensor target moves in the positive Z direction (Figure 8c). This flux density can be measured by inserting a Flux Density Sensing (FDS) Coil into the air gap as shown in Figure 8: the amplitude of the voltage induced on the coil terminals will be proportional to the amplitude of the flux linked to the coil, which, in turn, will be proportional to the flux density in the area of interest. For example, with the sensor target in the nominal position (Figure 8a), there are three flux lines linked to the FDS Coil. If the rotor is displaced in the negative Z-direction (Figure 8b), the number of the flux lines linked to the coil increases to four, and, conversely, if the rotor is displaced in the positive Z-direction (Figure 8c), the number of the flux lines linked to the coil reduces to two.

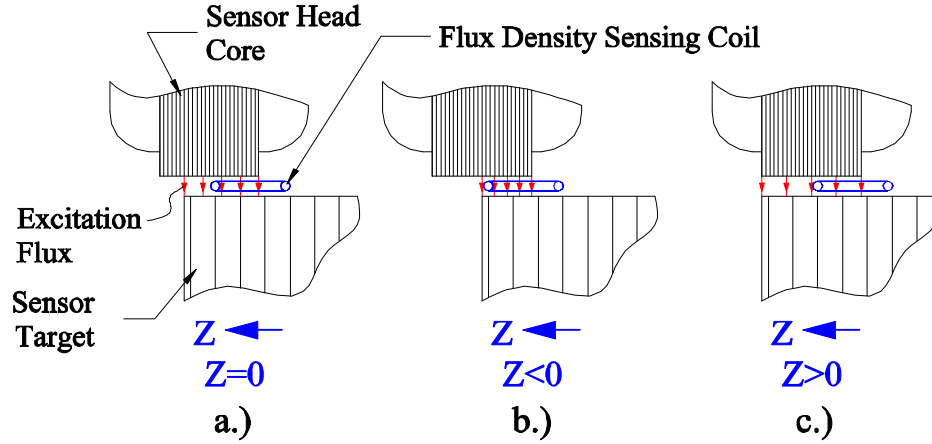


Figure 8: Illustration of the operational principle of the constant-flux edge sensor.

Figure 9 provides more details of the sensor construction and operation. In addition to soft-magnetic and electrically non-conductive Sensor Target Portion #1, it may also have a non-magnetic and electrically conductive Sensor Target Portion #2. An AC magnetic flux will be expelled from the Sensor Target Portion #2 due to the skin effect and concentrated in the Portion #1, forming a sharp flux edge at the boundary between the two portions.

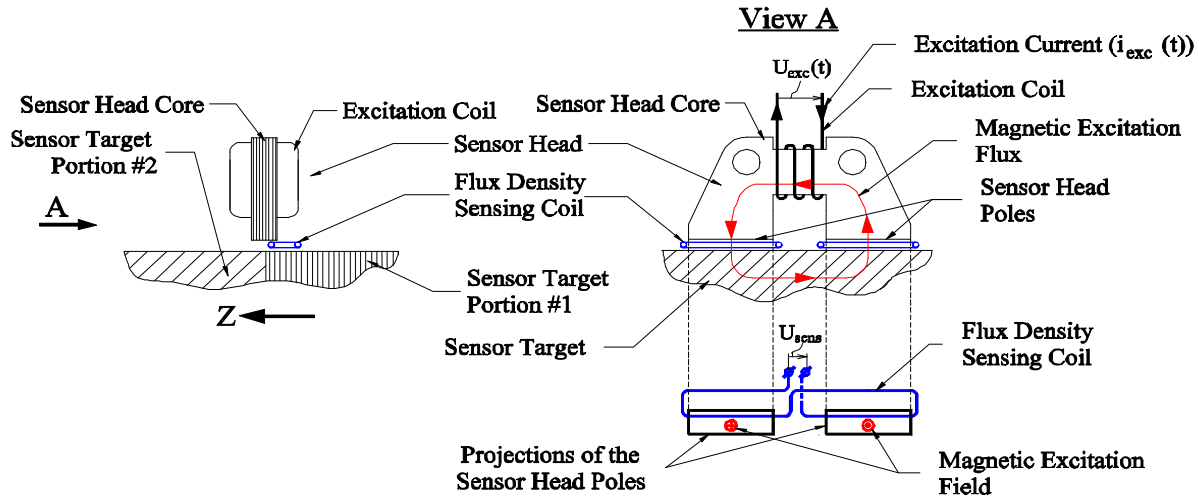


Figure 9: Details of the operation of the constant-flux edge sensor.

Figure 10 clarifies how the total excitation flux in the air gap is maintained constant. Figure 10a shows an equivalent electrical schematic for the excitation magnetic circuit of the sensor shown in Figure 9. An excitation current  $i_{exc}(t)$  flowing in the excitation coil of the sensor comprising  $N$  turns creates a magnetomotive force (MMF)  $N \cdot i_{exc}(t)$ , and, subsequently, induces a magnetic flux  $\Phi_{exc}(t)$ . The flux path is composed of the sensor head core, radial air gap and sensor target with associated magnetic reluctances  $R_{head}$ ,  $R_{gap}$  and  $R_{target}$  respectively.

Figure 10b shows an electrical schematic used to induce the current  $i_{exc}(t)$ . In contrast to electrical schematics shown in Figures 2, 3 and 4, there are no voltage dividers involved and the sensor excitation coil is directly connected to a source of excitation voltage  $U_{exc}(t)$ . Any periodic time profile of the voltage  $U_{exc}(t)$  can be used, such as square-wave, triangular, sinusoidal, etc, however the square-wave appears to be the most practical choice. According to Faraday's law, the excitation magnetic flux  $\Phi_{exc}(t)$  and the excitation voltage  $U_{exc}(t)$  are linked by the following equation:

$$U_{exc}(t) = N \frac{d\Phi_{exc}(t)}{dt} \tag{1}$$

An important outcome of a direct relation between  $\Phi_{exc}(t)$  and  $U_{exc}(t)$  is that if we maintain the amplitude of  $U_{exc}(t)$  constant, then the amplitude of  $\Phi_{exc}(t)$  will also stay constant regardless of values of  $R_{head}$ ,  $R_{gap}$  and  $R_{target}$ , which can be affected by the external fields, changes in the radial gap, etc.  $R_{head}$ ,  $R_{gap}$  and  $R_{target}$  will, however, affect the value of the excitation current  $i_{exc}(t)$  – the larger total value of the magnetic reluctance  $R_{total} = R_{head} + R_{gap} + R_{target}$ , the larger will be the amplitude of the excitation current. This can be also explained using a definition of the inductance of the excitation coil:

$$L = \frac{N \cdot \Phi_{exc}}{i_{exc}} = \frac{N^2}{R_{head} + R_{gap} + R_{target}} \quad (2)$$

Using (2), equation (1) can be presented in a well-known form:

$$U_{exc}(t) = L \frac{di_{exc}(t)}{dt} \quad (3)$$

where the inductance  $L$  changes when the air gap changes, or when the sensor target is displaced axially, or when the reluctance of the sensor head core changes because of an external magnetic field. For example, when the radial air gap between the sensor head core and the sensor target increases, the reluctance of the gap  $R_{gap}$  increases as well,

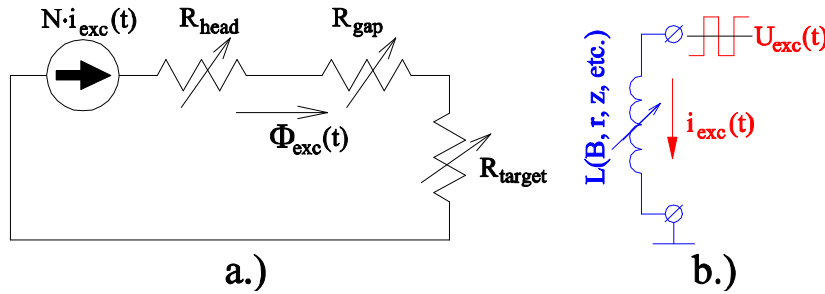


Figure 10: a.) Equivalent electrical schematic for the magnetic circuit; b.) An electrical schematic for the excitation coil.

the inductance of the excitation winding  $L$  decreases according to (2) and the amplitude of the excitation current  $i_{exc}(t)$  increases according to (3). The amplitude of the excitation flux  $\Phi_{exc}(t)$ , however, will remain constant driven by (1). Because of this feature the new sensor was given a name “a constant-flux edge sensor”.

Because the Sensor Target Portion #1 shown in Figure 9 can be made laminated, even at high operational frequencies there will be no significant eddy currents induced in it, which would otherwise negatively impact the sensor gain. Moreover, using a higher frequency may even result in a slightly higher gain because the fields would be better expelled from the conductive and non-magnetic Sensor Target Portion #2 producing a better “edge”. This is a big advantage over the sensor shown in Figure 3 where the sensor target is difficult to laminate and eddy currents induced in it result in a loss of the sensor gain at higher frequencies. Even though the sensor bandwidth is also affected by the signal processing electronics, a higher operational frequency of a sensor allows for a higher sensor bandwidth. Most AMB applications require sensor bandwidth in order of 3kHz, which is very easy to achieve and even exceed with the proposed sensor technology.

## 2 Prototype of the Constant-Flux Edge Sensor

Several prototypes of the constant-flux edge sensor have been built and evaluated during the sensor development. Figure 11 shows one of the latest prototypes, which actually was a complete combination sensor providing both axial and radial rotor position sensing using a single sensor target. This prototype was later used to replace conventional radial and axial sensors in a 330kW 37kRPM turbocompressor, which was successfully tested up to the full speed. Figure 11 shows a single-sided version of this sensor; later a differential version with similar dimensions was built and tested as well. The sensor assembly included two sets of edge sensor heads and FDS Coils located diametrically opposite from each other with the excitation windings connected in parallel and connected to a source of the excitation voltage of constant amplitude  $U_{exc}$ , whereas two FDS Coils were connected in series so that the voltages induced in them added to each other.

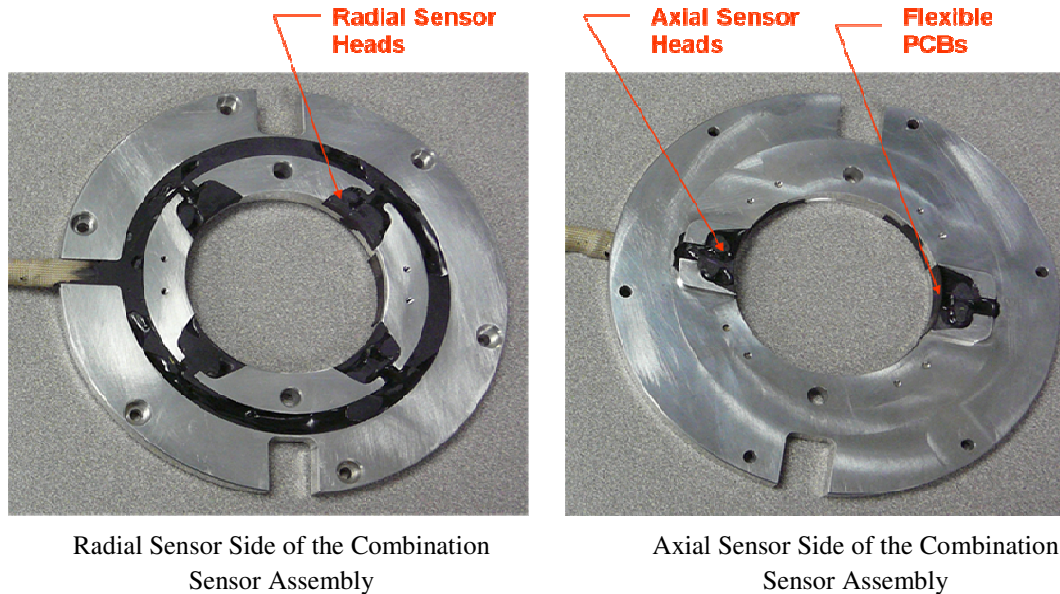


Figure 11: Prototype of a combination (axial and radial) sensor assembly with a single-sided constant-flux edge sensor.

The FDS Coils have been manufactured using Flexible PCB technology with a Kapton substrate. This technology is widely used in commercial products (e.g. to manufacture flexible ribbon cables), which makes FDS Coils very inexpensive. The traces on a Flexible PCB can easily be made as small as  $75\mu\text{m}$  wide with a  $75\mu\text{m}$  gap between them, which allows placing a very large number of turns per unit length. Since there is no current in the FDS coils, a high resistance due to a small cross-section of the traces is not important. An FDS coil manufactured with flexible PCB technology can be easily bent and glued to the inner diameter of the sensor assembly using an appropriate epoxy. Figure 12 shows an FDS coil used in the sensor prototype. The flexible PCB contained four layers and accommodated 156 turns.

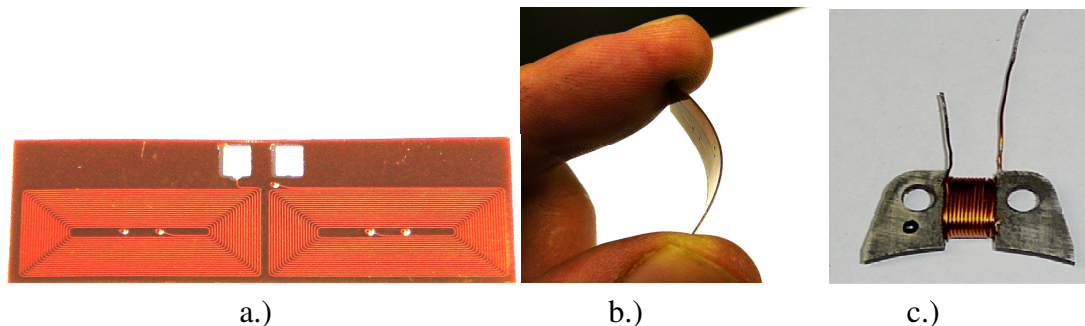


Figure 12: a.) Flux Density Sensing (FDS) Coil manufactured using flexible Printed Circuit Board Technology on a Kapton substrate. The printed circuit board has four layers accommodating total of 156 turns. b.) The circuit board can be easily bent to follow the inner diameter profile of the sensor housing. The PCB dimensions are  $29\text{mm} \times 10\text{mm} \times 0.38\text{mm}$ . c.) Laminated horse-shoe sensor head with excitation winding.

### 3 Sensor performance evaluation test setup description

The test rig shown in Figure 13 has been used to carry out axial sensor calibration and evaluate errors caused by radial displacements of the sensor target and external magnetic fields. Two orthogonal linear stages with graduated knobs seen in Figure 13 were used to move the sensor target either in the axial direction or in one of the radial directions. A set of axially magnetized permanent magnets mounted on a disk that can be moved along a threaded

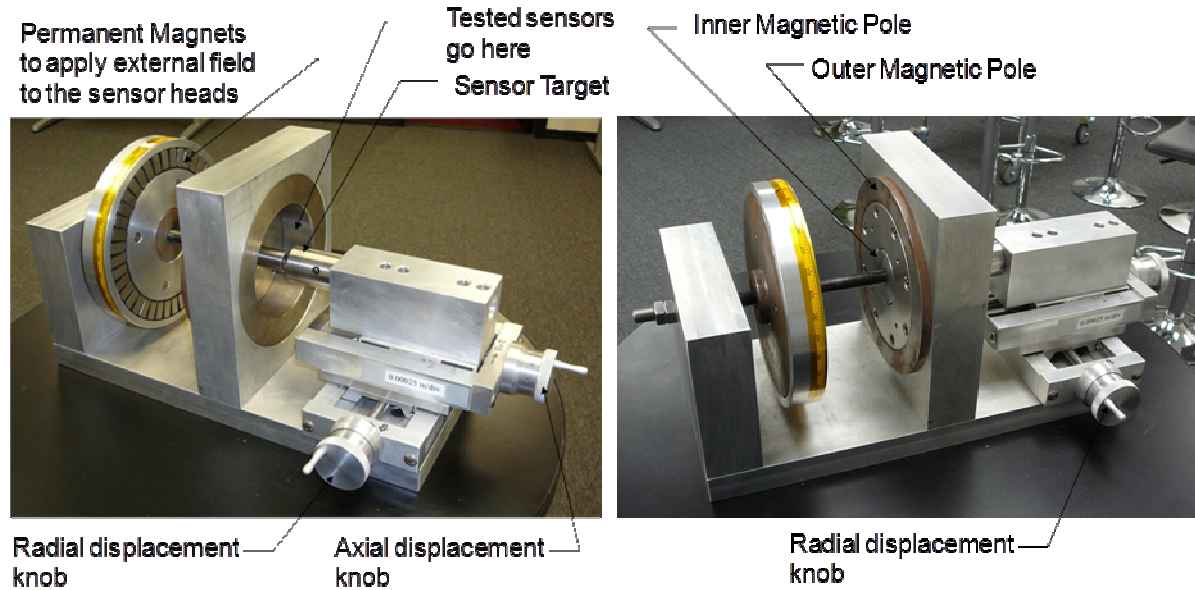


Figure 13: Test rig for sensor calibration and evaluation of errors caused by radial displacements and external magnetic fields.

rod closer to or further from the sensor assembly were used to apply variable external DC magnetic field to the sensor heads of the assembly. More details of how the external field was applied are given in Figure 14, which shows an axial cross-section of the test rig shown in Figure 13. The magnetic circuit for the external field generation included the above mentioned Permanent Magnets, cylindrical Outer and Inner Poles, Sensor Head Core, Sensor Target, Soft-Magnetic Portion of the Rotor, Inner Pole and the Magnetic Backiron. The Field Adjustment Disk was mounted on a threaded rod so that the gap between the disk and the outer and inner poles, and, consequently, the external magnetic field in the sensor heads could be changed by turning the disk. The rotor mockup was mounted on an X-Y table allowing it to be moved axially (Z-direction) and horizontally (X-direction).

Note that the sensor heads in Figure 14 are shown mounted in the vertical plane in order to make them visible in the vertical cross-section, whereas in reality they were mounted in the horizontal plane so that moving the rotor mockup in the X-direction would affect clearances between the sensor heads and the sensor target.

The test fixture for evaluating the temperature-induced errors of the constant-flux edge sensor is shown in Figure 15. The rotor mockup in the test fixture had been locked axially and radially in the nominal position with respect to the edge sensor. The entire fixture had been heated in an oven to a specified temperature with sufficient time given to achieve a thermal equilibrium at each data point. The sensor target retainer was always made out of non-magnetic stainless steel since it always served as one of the components defining "electromagnetic edge". The

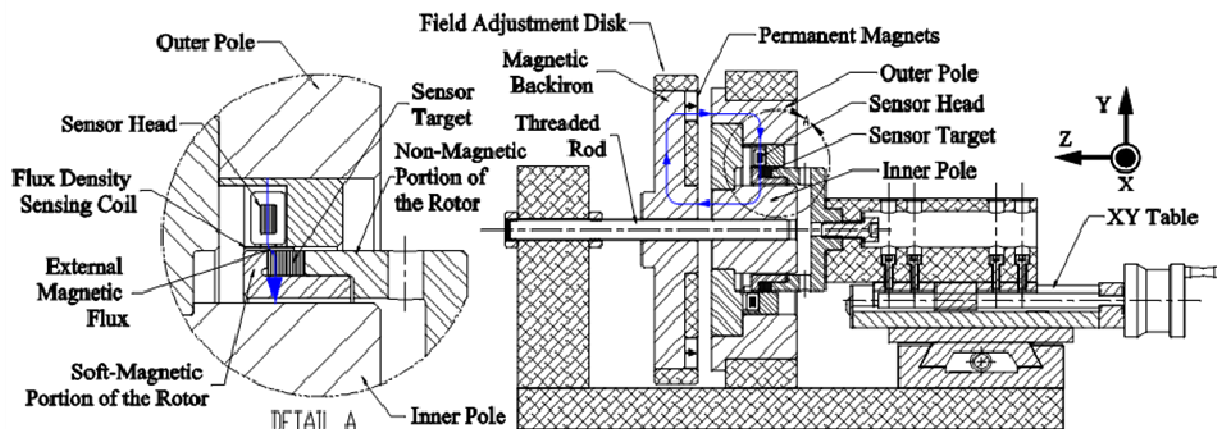


Figure 14: Schematic axial cross-section of the test rig shown in Figure 13. The sensor heads were located in a horizontal plane, but shown in the vertical plane to make them visible in the vertical cross-section.

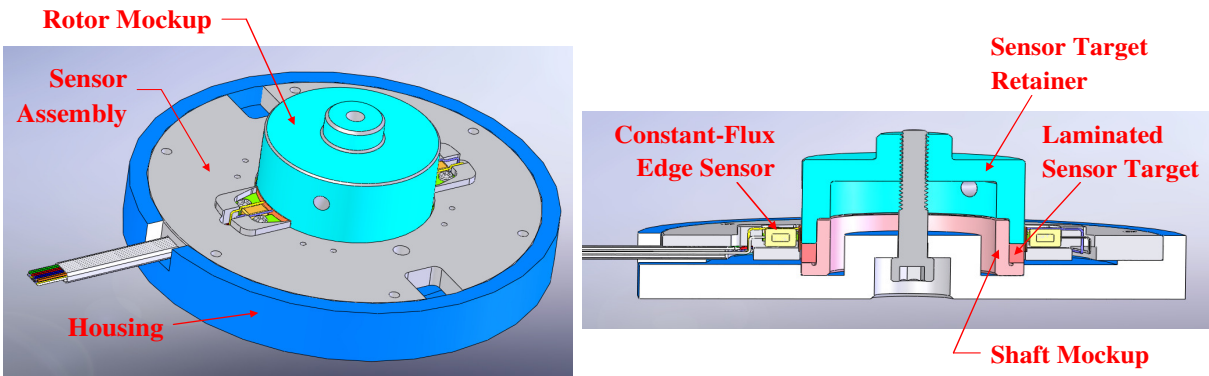


Figure 15: Test setup for evaluating the temperature-induced errors of the Constant-Flux Edge Sensor.

shaft mockup, on the other hand, was made out of a non-magnetic stainless steel for testing differential sensor configurations (where it also served as one of the components defining "electromagnetic edge") but both a non-magnetic stainless steel or a soft-magnetic carbon steel versions were used for testing single-sided sensor configurations.

### 3 Sensor performance evaluation test results

#### 3.1 Measurement range and linearity

A prototype of the constant-flux edge sensor exhibited a very large range of the target positions where the sensor output was changing monotonically with the target displacements (in excess of 5mm). The sensor output (after signal processing electronics) as a function of the sensor target position is shown in Figure 16. In the middle section of the curve shown in Figure 16, the raw sensor gain defined as change of the RMS voltage measured directly on the terminals of two FDS coils connected in series was in excess of 8V/mm (200V/in). With +/-0.38mm (+/-0.015in) displacement range from the nominal position, the new sensor offers a large range of nominal positions where the gain variations do not exceed 20%.

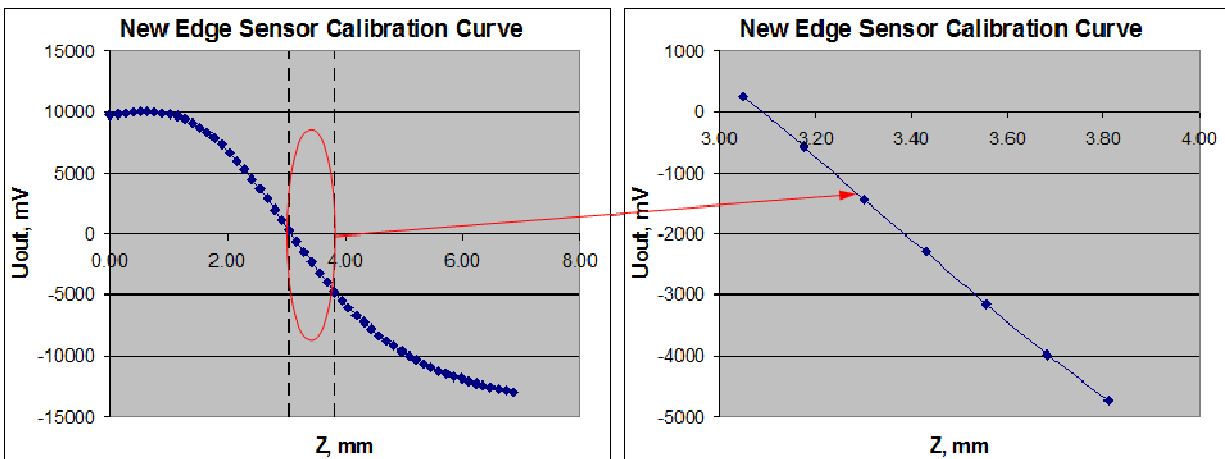


Figure 16: Measured calibration curve of the Constant-Flux Edge Sensor. The total measurement range was in excess of 5mm. There were many 0.75mm linear subranges such as shown on the right where the gain varied by less than  $\pm 20\%$ .

### 3.2 Errors induced by radial displacements of the rotor

Figure 17 illustrates an error caused by rotor radial displacements. As mentioned earlier, this error in the conventional edge sensors can be corrected based on the radial sensor readings, however, having a much smaller error in the constant-flux edge sensor eliminates the need for such corrections and simplifies the sensor use. An asymmetric character of this error for the constant-flux edge sensor indicates that it originates from differences in properties of two diametrically opposite sensor head – FSD coil assemblies.

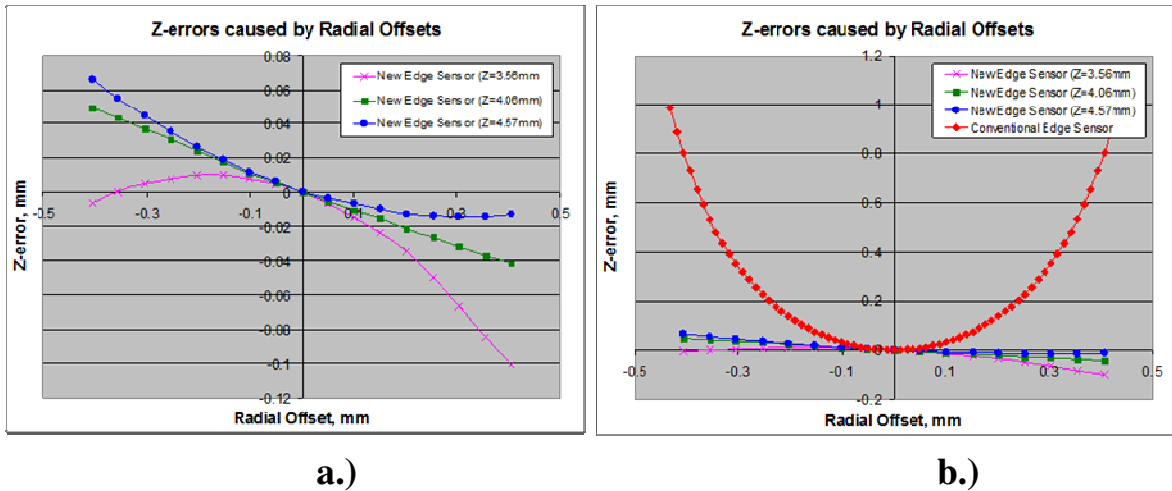


Figure 17: Axial position reading error as a function of the radial displacements of the sensor target a.) Constant-Flux Edge Sensor only; b.) Constant-Flux and a conventional edge sensor with similar dimensions, the errors curves are plotted on the same scale for comparison purposes.

### 3.3 Errors induced by external DC magnetic fields (leakage fields)

Figure 18 shows axial position measurement errors caused by external fields for several axial and radial positions of the sensor target. The field values indicated in Figure 18 have been measured with a Hall sensor inserted in the air gap between the sensor head poles and the sensor target. The errors observed with a conventional edge sensor utilizing the same sensor heads and tested on the same test rig are also shown for the comparison purposes. More than 20-time reduction of the error in high magnetic fields has been observed with the new constant-flux edge sensor compared to the conventional edge sensor.

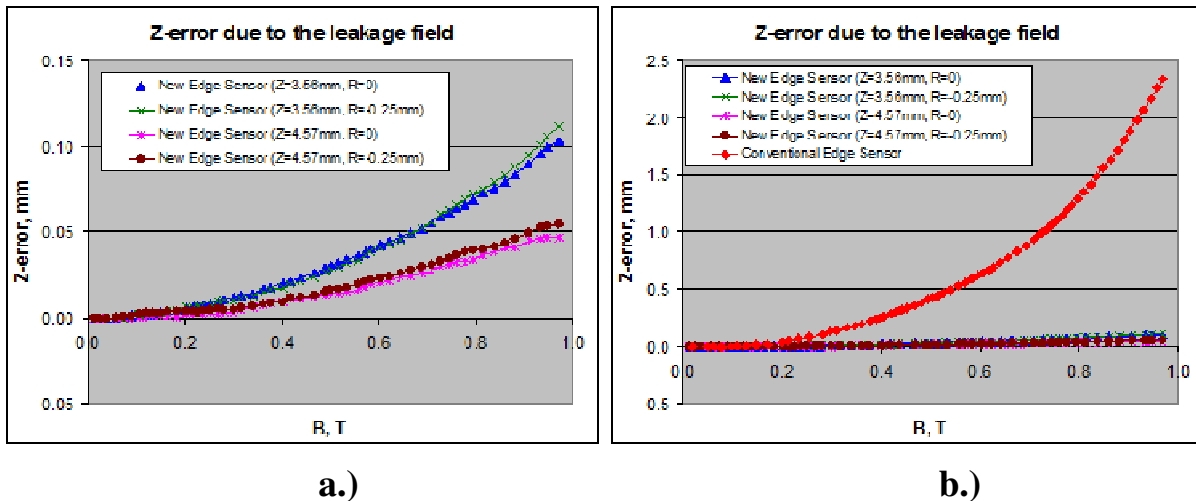


Figure 18: Axial position reading error as a function of the external DC magnetic field. a.) Constant-Flux Edge Sensor only; b.) Constant-Flux and a conventional edge sensor with similar dimensions; the errors curves are plotted on the same scale for comparison purposes.

### 3.3 Errors induced by temperature variations

The thermal errors were evaluated for both single-sided and differential sensor configurations using the setup shown in Figure 15. The entire fixture had been heated in an oven to a specified temperature with sufficient time given at each data point to achieve a thermal equilibrium. The results are presented in Figure 19. The differential sensor configuration clearly exhibit a superior thermal stability, making it a design choice for high-temperature applications. The temperature was limited in the experiment to 170°C only because of the temperature limit of available flexible PCBs, however higher-temperature flexible PCBs suitable for the temperatures up to 250°C have been already made and a higher-temperature version of a constant-flux edge sensor is expected to be tested in the nearest future.

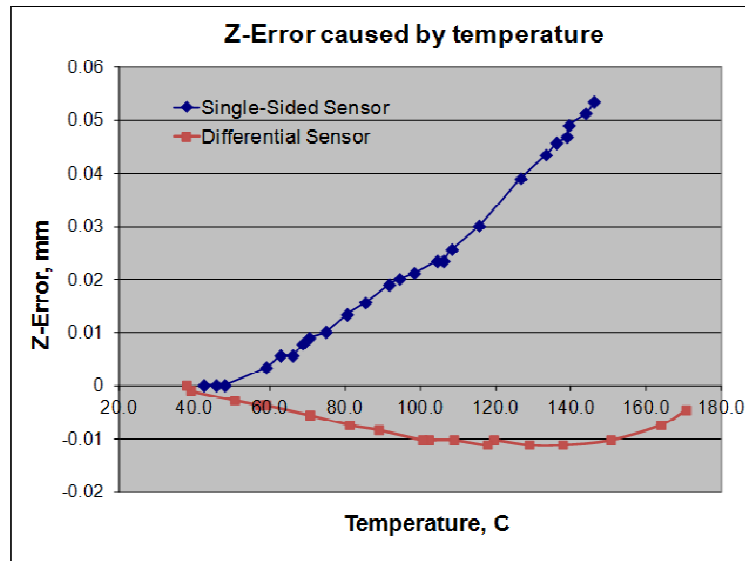


Figure 19: Temperature-induced axial position reading error.

## 4 Conclusions

A new design of an axial position sensor (constant-flux edge sensor) has been proposed and evaluated. The sensor offers a unique combination of advantageous properties not found collectively in other axial position sensing solutions, including:

1. Ability to work in dusty environments and in many working fluids.
2. Low sensitivity to external leakage fields.
3. Low sensitivity to radial rotor displacements.
4. Low sensitivity to temperature variations.
5. Large temperature operating range (up to 175°C tested, up to 250°C theoretically possible).
6. Excitation frequency in the ranges where impedance of the external wiring can be neglected, but the sensor bandwidth is sufficient for AMB applications (we use 25-50kHz excitation frequency).
7. Raw gain above 4.0 V/mm.
8. Very large total measurement range (in excess of 5mm).
9. Sufficiently large linear subranges (at least 0.75mm) where the gain variation does not exceed +/-20%. (There are many linear subranges within the total measurement range).
10. No requirements for a sensor target surface normal to the Z-axis.
11. Commonality with the radial sensor design.

The sensor functionality has been first validated through several static performance evaluation tests conducted on the sensor prototypes. These included evaluations of the total measurement range, linearity and magnitudes of errors caused radial displacements, external magnetic fields and temperature.

Later the sensor has been integrated into existing commercial machines on magnetic bearings - a 165kW 26.5kRPM Expander/Generator for Waste Heat Recovery [9], and 330kW 37kRPM gas compressor. Both machines have been successfully tested to their full operating speeds.

Currently the constant-flux edge sensor is a standard position sensing solution for all new Calnetix magnetic bearing systems. Recently built machines utilizing this sensor include 15.6kRPM 325kW turbocompressor and 16kRPM 250kW atomizer. Both machine have been successfully brought to the full speed and the turbocompressor has passed the entire in-house commissioning cycle.

## Nomenclature

Symbol	Meaning
B	Magnetic Flux Density
i	Current
L	Inductance
N	Number of Turns
R	Magnetic Reluctance
U	Voltage
$\Phi$	Magnetic Flux

## References

- [1] Editors: G. Schweitzer, and E. H. Maslen. *Magnetic Bearings*, Springer-Verlag, Berlin Heidelberg, 2009.
- [2] E. H. Maslen, T. Iwasaki, and R. Mahmoodian. Formal Parameter Estimation for Self-Sensing. In *10<sup>th</sup> International Symposium on Magnetic Bearings*, Martigny, Switzerland, August 2006.
- [3] S. Moriyama, W. Katsuhide, and H. Takahide. Inductive Sensing System For Active Magnetic Suspension Control. In *6<sup>th</sup> International Symposium on Magnetic Bearings*, Massachusetts, USA, pp. 529-537, August 1998.
- [4] L. Li. Eddy-Current Displacement Sensing Using Switching Drive When Baseband Sensor Output Is Readily Available. *IEEE Transactions on Instrumentation and Measurement*, Vol. 57, No. 11, pp. 2548-2553, 2008.
- [5] [www.kamansensors.com/html/technology/technology-tncablelength.htm](http://www.kamansensors.com/html/technology/technology-tncablelength.htm)
- [6] R. Larsonner and P. Buhler. New Radial Sensor for Active Magnetic Bearings. In *9<sup>th</sup> International Symposium on Magnetic Bearings*, Lexington, Kentucky, USA, August 2004.
- [7] P. McMullen, V. Vuong, and L. Hawkins. Flywheel Energy Storage System with AMB's and Hybrid Backup Bearings. In *10<sup>th</sup> International Symposium on Magnetic Bearings*, Martigny, Switzerland, August 2006.
- [8] L. Hawkins, P. McMullen, and V. Vuong. Development and Testing of the Backup Bearing System for an AMB Energy Storage Flywheel. In *ASME Turbo Expo 2007: Power for Land, Sea and Air*, Montreal, Canada, May 2007.
- [9] L. A. Hawkins, L. Zhu, and E. J. Blumber. Development of a 125kW Expander/Generator for Waste Heat Recovery. In *ASME Turbo Expo 2010: Power for Land, Sea and Air*, Glasgow, UK, June 2010.
- [10] P. T. McMullen, C. S. Huynh, and R. J. Hayes. Combination Radial-Axial Magnetic Bearing. In *7<sup>th</sup> International Symposium on Magnetic Bearings*, ETH, Zurich, Switzerland, pp. 473-478, August 2000.

## Acknowledgement

We would like to acknowledge patience and dedication that Magnetic Sensor Corporation ([www.magsensors.com](http://www.magsensors.com)) demonstrated in order to adopt production of the new sensors in a very timely manner.